

Primary Energy Spectra and Elemental Composition. GAMMA Experiment

S.V. Ter-Antonyan* and R.M. Martirosov, A.P. Garyaka, V. Eganov
Yerevan Physics Institute, 2 Alikhanyan Br. Str., 375036 Yerevan, Armenia

N. Nikolskaya, T. Episkoposyan
Moscow Lebedev Physics Institute, Russia

J. Procureur
Centre d Etudes Nucleaires de Bordeaux-Gradignan, Gradignan, France

Y. Gallant
Laboratoire de Physique Théorique et Astroparticules, Université Montpellier II, France

L. Jones
University of Michigan, Dept. of Physics, USA
(Dated: July 15, 2018)

On the basis of the Extensive Air Shower (EAS) data observed by the GAMMA experiment the energy spectra and elemental composition of the primary cosmic rays have been derived in the $10^3 \div 10^5$ TeV energy range. Reconstruction of the primary energy spectra is carried out in the framework of the SIBYLL and QGSJET interaction models and the hypothesis of the power-law steepening primary energy spectra. The obtained energy spectra of primary H, He, O, Fe nuclei along with the SIBYLL interaction model agree with the corresponding extrapolations of known balloon and satellite data at the $\sim 10^3$ TeV energies. The energy spectra obtained from the QGSJET model, show predominant proton composition of cosmic rays in the knee region. The evident rigidity-dependent behavior of the primary energy spectra for both interaction models are displayed at the following rigidities: $E_R \simeq 2400 \div 3000$ TV (SIBYLL) and $E_R \simeq 3400 \pm 200$ TV (QGSJET).

Using parametric event-by-event method of the primary energy evaluation by measured $N_{ch}, N_\mu(E_\mu > 5 GeV, R < 50m)$ and age (s) shower parameters, the all-particle energy spectra were obtained.

All presented results are derived taking into account the detector response, reconstruction uncertainties of EAS parameters and fluctuation of EAS development.

PACS numbers: 96.40.Pq, 96.40.De, 98.70.Sa

I. INTRODUCTION

The investigation of the energy spectra and elemental composition of primary cosmic rays in the knee region ($10^3 \div 10^5$ TeV) remains to be one of the intriguing problems of the modern high energy cosmic-ray physics. Despite the fact that these investigations have been carried out for more than half a century, the data on the elemental primary energy spectra at energies of $E > 10^3$ TeV need improvement. However, a bend of the all-particle energy spectra at around $3 \cdot 10^3$ TeV (called the "knee") at overall spectrum $\sim E^{-2.7}$ until the knee and $\sim E^{-3.1}$ beyond the knee, may be considered as an avowed fact. Moreover, assuming that the supernova explosion is the main source of the cosmic rays, different theoretical models of the high energy cosmic-ray origin and propagation through the Galaxy, predict the rigidity-dependent steep-

ening primary energy spectra in the knee region [1, 2, 3]. High statistical accuracies of the last EAS experiments [4, 5, 6] already allowed us to infer that the rigidity-dependent steepening energy spectra of primary nuclei can approximately describe the observed EAS size spectra in the knee region in the framework of conventional interaction models. However, the accuracies of the obtained elemental primary energy spectra are still insufficient due to both the uncertainty of interaction model and the accuracy of the solutions of the EAS inverse problem.

The Gamma facility (Fig. 1) was designed at the beginning of 90's in the framework of the ANI experiment [7] and the preliminary results of EAS investigations presented in [8, 9, 10, 11]. The main characteristic features of the GAMMA experiment are the mountain disposition, symmetric location of the EAS detectors and underground muon scintillation carpet that detects EAS muon components at $E_\mu > 5$ GeV energies.

Here, the description of GAMMA facility, EAS inverse approach determining the primary energy spectra using the observed EAS data, and main results of investigation

*Electronic address: samvel@yerphi.am;
URL: <http://gamma.yerphi.am/samvel/>

during 2002-2004 [10, 11] are presented in comparison with the corresponding MC-simulated data in the framework of the SIBYLL [12] and QGSJET [13] interaction models.

II. GAMMA EXPERIMENT

The GAMMA installation is a ground based array of 33 surface particle detection stations and 150 underground muon detectors located on the south side of Mount Aragats, Armenia. Elevation of the GAMMA facility is 3200 m above sea level, which corresponds to 700 g/cm² of atmospheric depth. The diagrammatic layout is shown in Fig. 1.

The surface stations of the EAS array are located on 5 concentric circles of radii: 20, 28, 50, 70, 100 m and each station contains 3 square plastic scintillation detectors with the following dimensions: 1x1x0.05 m³. Each of the central 9 stations contains an additional (4-th) small scintillator with dimensions 0.3x0.3x0.05 m³ (Fig. 1) for high particle density ($\gg 10^2$ particles/m²) measurements.

The photomultiplier tube is positioned on the top of the aluminum casing covering the scintillator. One of the three station's detectors is examined by two photomultipliers, one of which is designed for fast-timing measurements.

150 underground muon detectors (muon carpet) are compactly arranged in the underground hall under 2.3 Kg/cm² of concrete and rock. The dimensions, casing and applied photomultipliers are the same as in the EAS surface detectors.

A. Detector system and triggering

The output voltage of each photomultiplier is converted into the pulse burst by logarithmic ADC and transmitted to the CAMAC array where the corresponding electronic counters produce a digital number ("code") of pulses in the burst. Four inner ("trigger") stations are monitored by a coincidence circuit. If each of at least two scintillators of each trigger station detects more than 3 particles, the information from all detectors are then recorded along with the time between the master trigger pulse and the pulses from all fast-timing detectors. The given trigger condition provides EAS detection with the EAS size threshold $N_{ch} > (0.5 \div 1) \cdot 10^5$ at the location of the EAS core within the $R < 25$ m circle.

Before being placed on the scintillation casing, all photomultipliers are tested by a test bench using a luminodiode method where the corresponding parameters of logarithmic ADC and the upper limits $((0.5 \div 1) \cdot 10^4)$ of the measurement ranges are determined. The number of charged particles (n_i) passing through the i -th scintillator is computed using a logarithmic transformation: $\ln n_i = (C - C_0)/d$, where the scale parameter $d \simeq (9 \div 10) \pm 0.35$ is preliminarily determined by the test

bench, $C = (0 \div 2^7 - 1)$ is an output digital code from the CAMAC array corresponding to the energy deposit of n charged particles into the scintillator, $C_0 \simeq (5 \div 6) \pm 0.25$ is determined for each hour of run and is equal to the mode of the background single particle digital code spectra (Fig. 2).

The time delay $\Delta t_j = t_j - t_1$ of each j -th ($j = 2, \dots, 33$) fast timing detector is estimated by the pair-delay method [14] at the resolution time about $4 \div 5$ ns.

B. Reconstruction of EAS parameters

EAS zenith angle (θ) is estimated on the basis of measured shower front arrival times by 33 fast-timing surface detectors, applying the maximum likelihood method and flat-front approach [14, 15]. The corresponding uncertainty are tested by MC simulations and is equal to: $\sigma(\theta) \simeq 1.5^\circ$.

The reconstruction of the EAS size (N_{ch}), shower age (s) and core coordinates (x_0, y_0) are performed based on the NKG approximation of measured charged particle densities ($\{n_i\}, i = 1, \dots, m$) using the χ^2 minimization to estimate x_0, y_0 and the maximum likelihood method to estimate the N_{ch} taking into account the measurement errors. The logarithmic transformation $L(n_i) = \ln n_i - (1/m) \sum \ln n_i$ at $n_i \neq 0$, allows to obtain the analytical solution for the EAS age parameter (s) at the χ^2 minimization [15, 16]. Unbiased ($< 5\%$) estimations of N_{ch}, s, x_0, y_0 shower parameters are obtained at $N_{ch} > 5 \cdot 10^5$, $0.3 < s < 1.6$, and $R < 25$ m from the shower core to the center of the EAS array distances. Corresponding accuracies are derived from MC simulations by the CORSIKA(EGS) [17] and are equal to: $\Delta N_{ch}/N_{ch} \simeq 0.1$, $\Delta s \simeq 0.05$, $\Delta x, \Delta y \simeq 0.5 \div 1$ m.

The reconstruction of the total number of EAS muons (N_μ) by the detected muon densities ($\{n_{\mu,j}\}, j = 1, \dots, 150$) from the underground muon hall is carried out by restricting the distance $R_\mu < 50$ m from the shower core (so called "truncated" EAS muon size [20]) and Greisen approximation of the muon lateral distribution function: $\rho_\mu(r) = cN_\mu(R < 50m) \exp(-r/r_0)/(r/r_0)^{0.7}$, where $r_0 = 80$ m, $c = 1/2\pi \int_0^{50} \rho(r)rdr$. The truncated muon size $N_\mu(R < 50m)$ is estimated at known (from the EAS surface array) shower core coordinates in the underground muon hall. The unbiased estimations for muon size are obtained at $N_\mu > 10^3$ using the maximum likelihood method and assuming Poisson fluctuations of detected muon numbers. The reconstruction accuracies of the truncated muon size are equal to $\Delta N_\mu/N_\mu \simeq 0.2 \div 0.35$ at $N_\mu \simeq 10^5 \div 10^3$ respectively. Notice, that the detected muons in the underground hall are always accompanied by the electron-positron equilibrium spectrum which is produced when muons pass through the matter (2300 g/cm²) over the scintillation carpet. Since this spectrum depends on the muon energy ($\sim \ln E_\mu$), overestimations ($\sim 25 \div 30\%$) of the reconstructed muon size have to depend on the primary energy

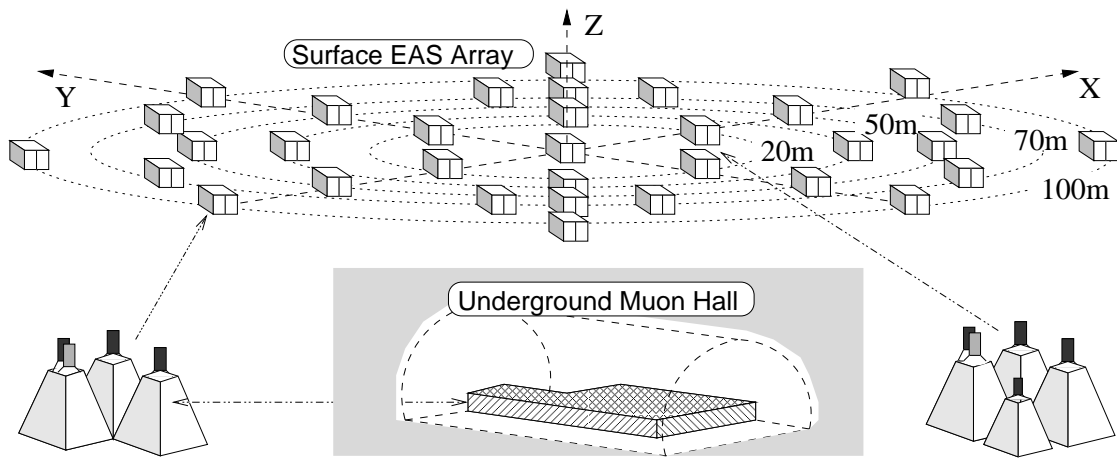


FIG. 1: Diagrammatic layout of the GAMMA facility

and therefore on the EAS size.

III. EAS SIMULATION

A. Key assumptions

All observed quantities ($\Delta F/\Delta\tilde{q}_u$) in the high energy EAS physics are obtained via convolutions of the energy spectra dI_A/dE of primary nuclei ($A \equiv H, He, \dots$ at least up to Ni) with the differential spectra $W_A(E, q_u)$ of the EAS parameters $q_u \equiv N_{ch}, N_\mu, s$ at the observation level and EAS array response functions $\partial\mathcal{R}_A(E, q_u, \theta)/\partial\tilde{q}_u$:

$$\frac{\Delta F_u}{\Delta\tilde{q}_u} = \frac{1}{C} \sum_A \int_E \frac{dI_A}{dE} \int_D \int_{Q_u} W_A(E, q_u) \frac{\partial\mathcal{R}_A}{\partial\tilde{q}_u} dE dD dq_u, \quad (1)$$

where the EAS parameter \tilde{q}_u is a reconstructed value of the corresponding parameter q_u on the observation level, $dD \equiv \cos\theta dx dy d\Omega$ is an element of the multidimensional phase space (D) of the EAS detection taking into account the EAS selection criteria and trigger conditions, $W_A(E, q_u, \theta)$ are the corresponding differential spectra of the EAS parameters (q_u) at the primary energy E , zenith angle of incidence θ and a given kind of primary nucleus (A), C is a corresponding normalization factor. In the general case, W_A depends on the interaction model [18, 19].

The multidimensional integral above is better to calculate by Monte-Carlo simulation, especially since the spectra $W_A(E, q_u, \theta)$ can be computed more or less precisely only by 3-dimensional EAS simulations.

B. Simulation scenario

We have computed the shower spectra $dW_A(E, q_u, \theta)$, ($q_u \equiv N_{ch}, N_\mu, s, \dots$) on the observation level of the

GAMMA facility using the CORSIKA6031(NKG,EGS) EAS simulation code [17] with the QGSJET01 [13] and SIBYLL2.1 [12] interaction models for 4 groups ($A \equiv H, He, O, Fe$) of primary nuclei at the power-law energy spectra ($\sim E^{-1.5}$) in the $5 \cdot 10^2 \div 5 \cdot 10^5$ TeV energy range. The spectral index (-1.5) was chosen to provide high statistical accuracies of the simulated data beyond the knee. The EGS mode of the CORSIKA was used for computations of the response functions of the GAMMA detectors taking into account the EAS gamma-quanta contributions and the choice of the corresponding input parameters of the adequate NKG mode.

Each EAS particle (γ, e, μ, h) obtained from the CORSIKA(EGS) on the observation level (not interrupting the CORSIKA routine) is passing through the steel casing (1.5 mm) of detector station and then through the corresponding scintillator. The pair production and Compton scattering processes are additionally simulated in the case of the EAS γ -quanta passing through the steel casing and the scintillator.

The resulting energy deposit in the scintillator is converted to the ADC code and inverse decoded into a number of "detected" charge particles taking into account all uncertainties of the ADC parameters (C_0, d) and the fluctuation of the light collected by the photomultiplier ($\sigma_l \simeq 0.25/\sqrt{n}$).

Using the simulation scenario above, 100 EAS events were simultaneously simulated by the CORSIKA routine at the EGS and NKG modes for $A \equiv H, He, O, Fe$ primary nuclei at log-uniform energy spectra in the $5 \cdot 10^2 \div 10^5$ TeV energy range. The computations of the charged particle densities in the surface detectors at NKG mode of the CORSIKA were performed by applying the two-dimensional interpolations of the corresponding particle density matrix from the CORSIKA routine [17]. The agreement ($\sim 5\%$) of the EGS and NKG simulated data was attained at the $E_e \simeq 1 \pm 1$ MeV kinetic energy threshold of the EAS electrons (positrons) at NKG mode (input parameter of CORSIKA code). However,

the energy threshold for the detection of a vertical single minimal ionizing background particle by scintillation counters is about $8 \div 9$ MeV and differences obtained by the CORSIKA NKG prediction are completely explained by contribution of EAS γ -quanta.

Thus, the EAS simulations by the CORSIKA with fast computation NKG mode at $E_e > 1$ MeV is adequate to the EAS simulation by the EGS mode taking into account the EAS γ -quanta and peculiarity of the GAMMA surface array.

All EAS muons with energies of $E_\mu > 4$ GeV on the GAMMA observation level have passed through the 2.3 Kg/cm² of rock to the muon scintillation carpet (the underground muon hall). Fluctuations of the muon ionization losses and electron (positron) accompaniment due to the muon bremsstrahlung, direct pair production, knock on and photo-nuclear interactions are taken into account. The transformation of the energy deposit to the number of detected muons is performed the same way as for the surface detectors.

The EAS simulations were performed at $4.5 \cdot 10^4$ primary H , $4.3 \cdot 10^4$ He , $2.4 \cdot 10^4$ O , $2.4 \cdot 10^4$ Fe nuclei using the CORSIKA NKG routine at the SIBYLL interaction model. Corresponding statistics at the QGSJET interaction model were: $4.1 \cdot 10^4$, $4.2 \cdot 10^4$, $2 \cdot 10^4$, $2 \cdot 10^4$. The energy thresholds of primary nuclei were the same for both interaction models and were set 0.5, 0.7, 1, 1.2 PeV respectively at $5 \cdot 10^3$ PeV upper energy limit.

IV. MEASUREMENT ERRORS AND DENSITY SPECTRA

The close disposition of $k = 1, 2, 3$ scintillators in each of the (i -th) detector station of the GAMMA surface array allows to auto-calibrate the measurement error by detected EAS data. The measured and simulated particle density divergences $(n_k - \rho)/\rho$ versus average value $\rho = (1/3) \sum n_k$ at $R_i > 10$ m distances from shower core are shown in Fig. 2 (circle symbols). The obtained dependences are completely determined by Poisson fluctuations (at $R_i \gg 1$ m) and measurement errors.

The agreement of the measured and simulated dependences allowed to extract the real measurement errors of the GAMMA detectors. In Fig. 2 the corresponding results are shown (square symbols).

The background single particle spectra (in the units of ADC code) detected by GAMMA surface scintillators for 78 sec operation time are shown in Fig. 3 (dotted lines). The background single particle spectra detected by underground muon scintillators have the same shape at about 10 times less intensities.

These spectra are used for the operative (each hour) determination of ADC parameters (C_0) during an experiment. The symbols and solid lines in Fig. 3 display the corresponding expected spectra obtained by MC-simulation taking into account the measurement errors (symbols) and without errors (line) respectively. The

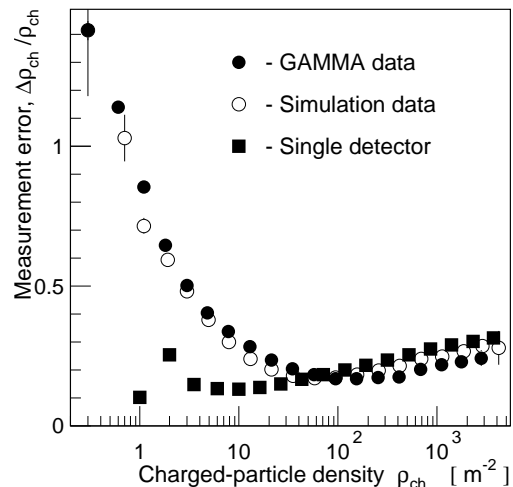


FIG. 2: Particle density divergences (circle symbols) and measurement error of single detector (square symbols) versus charged-particle density.

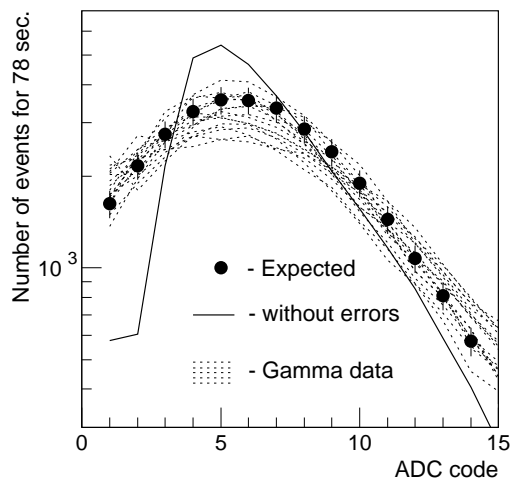


FIG. 3: Background single particle spectra of 15 surface detectors (dotted lines). The symbols (solid line) are the expected spectra taking into account (without) measurement errors.

minimal primary energy in simulation of the background particle spectra was confined to the 7.6 GV primary particle's geomagnetic rigidity.

Because the effective primary energies responsible for the single particle spectra at observation level 700 g/cm² are about ~ 100 GeV and the energy range is studied by direct measurements in the balloon and satellite experiments, the primary energy spectra and elemental composition at MC-simulation were taken from approximations [21]. Notice, that the expected single particle spectra at these energies are practically the same for QGSJET and SIBYLL interaction models.

Fig. 4a,b (symbols) display the charged particle density

spectra detected by the corresponding surface detectors (a) and underground muon detectors (b) at $R_i < 50$ m and different EAS size thresholds: $N_{ch} > 5 \cdot 10^5$, $N_{ch} > 10^7$ (and additionally $N_{ch} > 2 \cdot 10^6$ for muon density spectra).

The showers were selected at $\theta < 30^\circ$ and the shower core location in the $R < 25$ m range from center of the GAMMA facility (Fig. 1). The corresponding expected spectra (lines) at different interaction models are also shown in Fig. 4. The primary energy spectra and elemental composition at MC-simulations were taken from EAS inverse problem solution (see below). There is a good agreement of the expected and observed data for the surface array in the measurement range (about four orders of magnitude). However, the agreement of the detected muon density spectra with expected ones is attained only in the $N_{ch} < 10^7$ range. The observed discrepancies for the muon density spectra at $N_{ch} > 10^7$ are unaccounted for the present and demand subsequent investigations.

V. EAS DATA

The main EAS data of the GAMMA experiment are shown in Fig. 5-10 (symbols). These results were obtained at the $6.19 \cdot 10^7$ sec operation time and following selection criteria: $N_{ch} > 5 \cdot 10^5$, $R < 25$ m, $\theta < 30^\circ$, $0.3 < s < 1.6$. All the lines and shaded areas in Fig. 5-10 correspond to the expected spectra according to the QGSJET and SIBYLL interaction models.

The EAS size spectra ($N_{ch}^{2.5} \cdot dF(\theta)/dN_{ch}$) at 3 zenith angular intervals are shown in Fig. 5. The truncated muon size spectra in the same zenith angular intervals are shown in Fig. 6. These spectra normalized to the EAS intensity at $N_{ch} > 5 \cdot 10^5$ and $\theta < 30^\circ$. The EAS size spectra at $\theta < 30^\circ$ and different thresholds of the truncated EAS muon size are shown in Fig. 7. The normalized EAS truncated muon size spectra at different EAS size thresholds are shown in Fig. 8. Fig. 9 displays the average EAS age parameter dependence on EAS size. The lines are the expected dependences according to QGSJET (dotted line) and SIBYLL (solid line) models. The obtained $N_\mu(N_{ch})$ dependences and corresponding expected values at the primary Hydrogen, Iron and mixed compositions computed in the frame of the SIBYLL and QGSJET interaction models are plotted on Fig. 10.

VI. EAS INVERSE PROBLEM AND PRIMARY ENERGY SPECTRA

A. Combined approximations of EAS data

Direct computations of the expected EAS spectra using the integral expression (1) is possible only in the framework of a given interaction model and known primary energy spectra. Moreover, the Gamma data shown

in Fig. 4-10 may only formally compare with the same data obtained by other EAS experiments performed at both similar atmospheric depths [15, 22, 23] and depths close to the sea level [4, 5, 24]. The correct comparison is possible only at known primary energy spectra and known interaction model because both transformation of the detected EAS spectra to the spectra at a given observation level and the extrapolation of the obtained spectra to another atmosphere depth in a general case are folded by the integral expressions similar to (1).

In such case the more reliable way to interpret the experimental data is to unfold the integral expression (1) at a given interaction model. As a criterion of the validity of the solutions, the χ^2 test of the detected and expected data may be performed. The agreement between the obtained energy spectra at different primary nuclei and the corresponding extrapolations of known balloon and satellite data to the given measurement range will also validate the solutions.

Evidently, the accuracies of the unfolding of expression (1) depend not only on number of measurement points (bins) and different measured spectra but also on the wealth of information about the primary energy spectra and the interaction model involved in the given measured EAS spectra. The amount of information contained in the expression (1) reveals itself via stability and uncertainties of the solutions.

It is shown in [26], that the EAS size spectra and EAS truncated muon size spectra at three zenith angular intervals allow to reliably unfold expression (1) at a given interaction model for not more than 2 kinds of primary nuclei. The unreliability of solutions of (1) for 4 kinds of primary nuclei was shown in [27], as well.

Taking into account the above, we used the parameterization of the integral equation (1) similar to [19, 28]. The solutions for the primary energy spectra in (1) were sought based on the theoretically known power-law function [2] with the "knee" at the rigidity-dependent energies $E_k(A) = E_R \cdot Z$ and the same indices ($-\gamma_1$) and ($-\gamma_2$) before and after the knee respectively, for all kinds of primary nuclei (A):

$$\frac{dI_A}{dE} = \Phi_A E_k^{-\gamma_1} \left(\frac{E}{E_k}\right)^{-\gamma} \quad (2)$$

where $\gamma = \gamma_1 \equiv 2.65$ at $E \leq E_k(A)$, $\gamma = \gamma_2$ at $E > E_k(A)$, E_R is particle's rigidity and Z is a charge of A nucleus.

Thus, the integral equation (1) is transformed into a parametric equation with unknown spectral parameters: $\Phi(A)$, $E_k(A)$, γ_2 , which are determined by minimization of χ^2 function:

$$\chi^2 = \frac{1}{\sum V_u} \sum_1^U \sum_1^{V_u} \frac{(\zeta_{u,v} - \xi_{u,v})^2}{\sigma^2(\zeta_{u,v}) + \sigma^2(\xi_{u,v})} \quad (3)$$

where U is the number of examined functions $\zeta_{u,v} \equiv \Delta F_u / \Delta \tilde{q}_{u,v}$ (Fig. 5-10, symbols) obtained from the experiment with statistical accuracies $\sigma(\zeta_{u,v})$

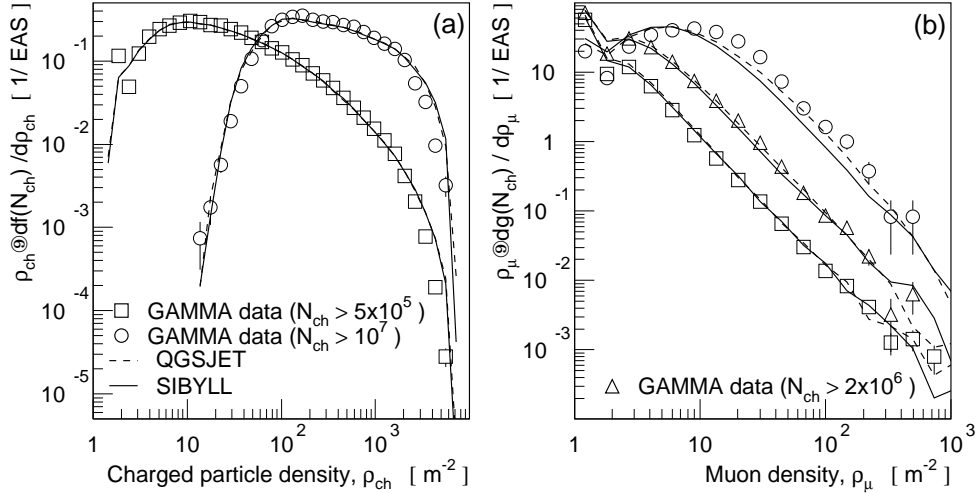


FIG. 4: Detected (symbols) and expected (lines) particle density spectra of surface scintillators (left panel, a) and underground muon scintillators (right panel, b).

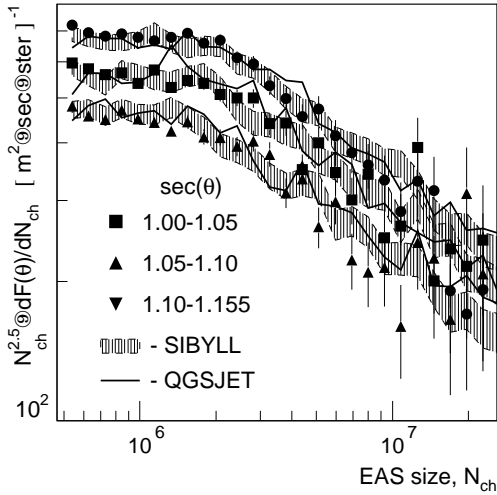


FIG. 5: EAS size spectra at 3 zenith angular intervals (symbols) and corresponding expected spectra according to the SIBYLL (shaded area) and QGSJET interaction models (lines).

at $v = 1, \dots, V_u$ measured points (bins), and $\xi_{u,v}$ and $\sigma(\xi_{u,v})$ are the corresponding expected values of the examined data set.

Using the aforementioned formalism and $U = 6$ 2-dimensional examined functions from Fig. 5-8 (symbols) and 1-dimensional functions from Fig. 9,10, the unknown spectral parameters $\Phi(A)$, $E_k(A)$, γ_2 were derived by the minimization of χ^2 function (3) at $\gamma_1 = 2.65$ and the degree of freedom $\sum_1^6 V_u \simeq 350$.

The values of spectral parameters (2) obtained by the solution of the parameterized equation (1) are presented in

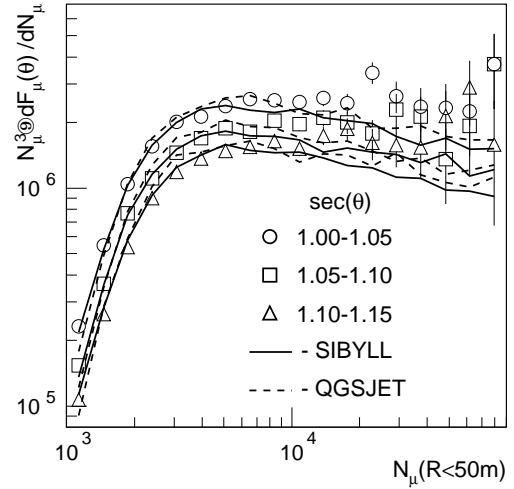


FIG. 6: Normalized EAS truncated muon size spectra at 3 zenith angular intervals (symbols). The lines correspond to the expected spectra at the SIBYLL (solid) and QGSJET (dashed) interaction models.

Table 1 at the QGSJET and SIBYLL interaction models. The derived primary energy spectra for p, He, O, Fe nuclei are shown in Fig. 11 (shaded areas) in comparison with the KASCADE data (symbols) from [25].

The expected spectra conforming the examined data set according to the solutions above are shown in Fig. 5-10 (lines and shaded area) for the QGSJET and SIBYLL interaction models. It is necessary to note, that the obtained results in the framework of the SIBYLL interaction model are more consistent and slightly dependent on a number of examined functions.

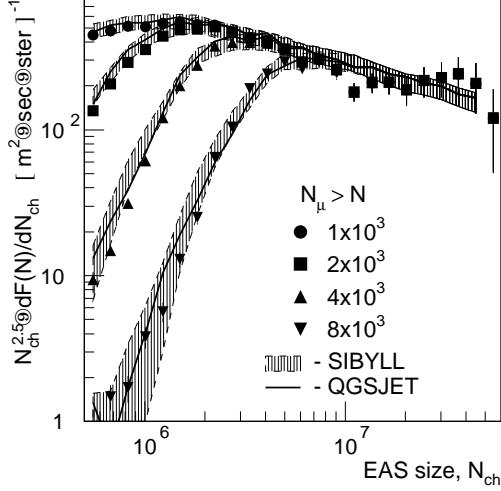


FIG. 7: EAS size spectra (symbols) at different truncated muon size thresholds and $\theta < 30^\circ$. The lines and shaded areas are the expected spectra according to the QGSJET and SIBYLL interaction models.

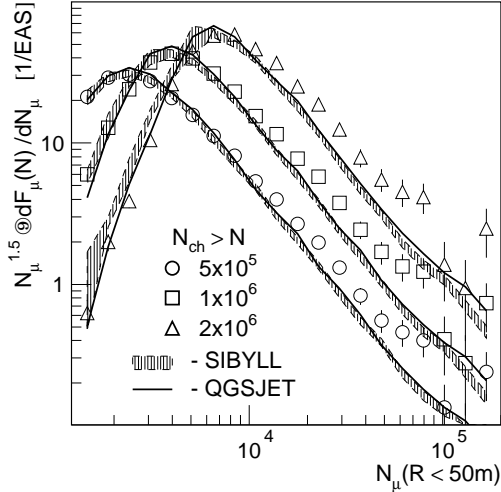


FIG. 8: Normalized EAS truncated muon size spectra at different EAS size thresholds (symbols). The lines and shaded areas correspond to the expected spectra at the QGSJET and SIBYLL interaction models respectively.

B. 4-Dimensional approach

The combination of 1,2-dimensional approximations of EAS data above does not take into account all the information about primary energy spectra folded in the detected EAS data. In general, the EAS inverse problem can be formulated in the multidimensional space of EAS parameters. In case of the 4-parametric $(N_{ch}, N_\mu, s, \theta)$

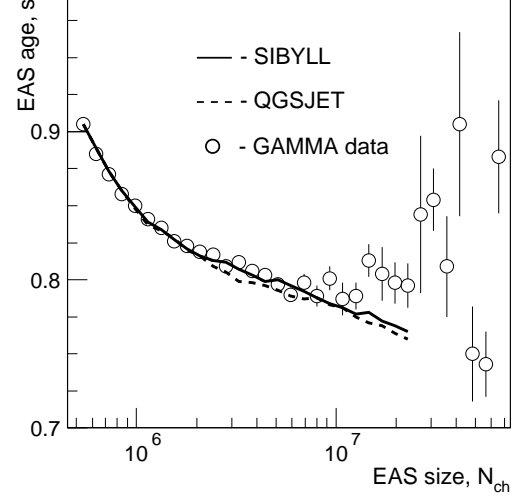


FIG. 9: Dependence of average EAS age parameter on EAS size.

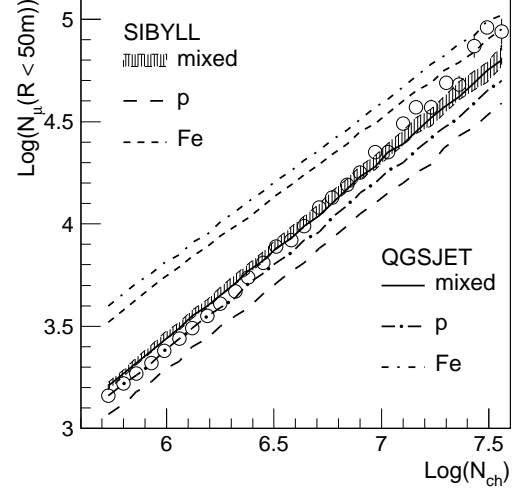


FIG. 10: Average EAS truncated muon size $N_\mu(E > 5 \text{ GeV}, R < 50\text{m})$ versus EAS size (N_{ch}). The dashed lines and shaded area are the expected dependences at the SIBYLL interaction models and pure p , Fe and mixed compositions respectively. Dash-dotted and solid lines are the same dependences at the QGSJET models.

analysis, the expression (1) is written as:

$$\frac{\Delta F}{\Delta \tilde{N}_{ch} \Delta \tilde{N}_\mu \Delta \tilde{s} \Delta \Omega} = \frac{1}{C} \sum_A \int_E \frac{dI_A}{dE} \int_Q \int_D \mathcal{G}_A(E, \theta) \times \mathcal{R}(\theta) dE dD dN_{ch} dN_\mu ds, \quad (4)$$

where $\mathcal{G}_A(E, \theta) \equiv \partial^3 W_A(E, \theta) / \partial N_{ch} \partial N_\mu \partial s$, are the multidimensional differential EAS spectra at given A, E, θ parameters of the primary nucleus, $\mathcal{R}(\theta) \equiv \partial^3 R(\theta) / \partial \tilde{N}_{ch} \partial \tilde{N}_\mu \partial \tilde{s}$ are the error functions of the experiment. The parameters with a tilde symbol are the

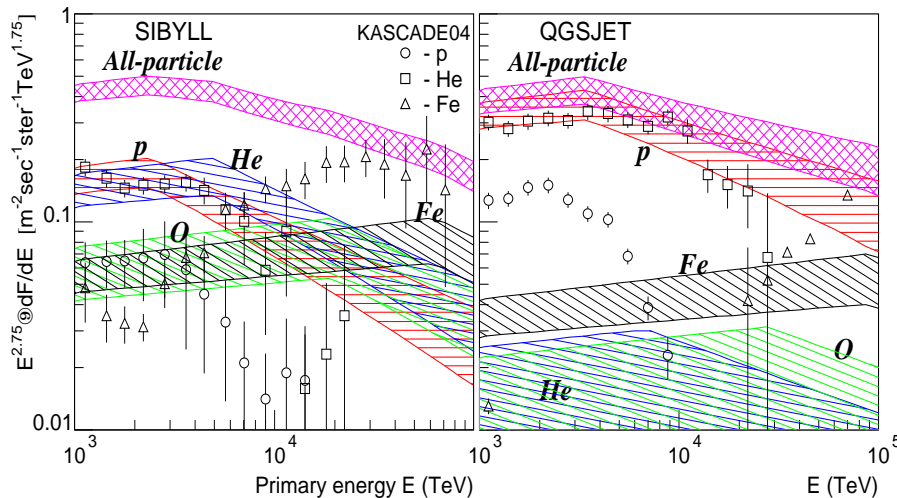


FIG. 11: Energy spectra and abundance of the primary nuclei (shaded areas) at the SIBYLL (left panel) and QGSJET (right panel) interaction models. The symbols are the KASCADE data from [25].

TABLE I: Parameters of primary energy spectra (2) at 1,2-dimensional analysis of EAS data. Scale factors Φ_A and particle's rigidity E_R have units of $(m^2 \cdot sec \cdot ster \cdot TeV)^{-1}$ and (TV) respectively.

Parameters	SIBYLL	QGSJET
Φ_H	0.081 ± 0.004	0.164 ± 0.004
Φ_{He}	0.072 ± 0.008	0.005 ± 0.008
Φ_O	0.028 ± 0.008	0.005 ± 0.006
Φ_{Fe}	0.028 ± 0.003	0.018 ± 0.003
E_R	2560 ± 200	3400 ± 150
${}^a\gamma_1$	2.65	2.65
γ_2	3.21 ± 0.04	3.10 ± 0.03
χ^2	2.5	2.6

^aParameter was fixed.

reconstructed values of corresponding EAS parameters. Evidently, the amount of information about primary energy spectra contained in the detected multidimensional spectrum ΔF is always greater than the cumulative amount of information contained in the 1,2-dimensional spectra $\Delta F_u / \Delta \tilde{q}_u$, $\tilde{q}_u \equiv \tilde{N}_{ch}, \tilde{N}_\mu, \tilde{s}$ of the expression (1). The difference is determined by the inter-correlations of EAS parameters that are taken into account in the expression (4).

On the basis of the EAS data set of the GAMMA experiment, the simulated EAS database (section III) and parameterization (2), the equations (4) were resolved by the χ^2 -minimization method. The computations were performed at the following bin dimensions: $\Delta \ln N_{ch} = 0.15$, $\Delta \ln N_\mu = 0.25$, $\Delta \sec \theta = 0.05$ and $\Delta s = 0.15$ on the left and right hand side of $s^* = 0.85$ and $\Delta s = 0.3$ in other cases. The total number of the degree of freedom at 4-dimensional χ^2 -minimization was equal to 1560.

The values of spectral parameters (2) obtained by the so-

TABLE II: Parameters of primary energy spectra (2) at 4-D analysis of EAS data. Scale factors Φ_A and particle's rigidity E_R have units of $(m^2 \cdot sec \cdot ster \cdot TeV)^{-1}$ and (TV) respectively.

Parameters	SIBYLL	QGSJET
Φ_H	0.089 ± 0.003	0.14 ± 0.004
Φ_{He}	0.053 ± 0.005	0.034 ± 0.004
Φ_O	0.049 ± 0.004	0.016 ± 0.003
Φ_{Fe}	0.029 ± 0.003	0.015 ± 0.002
E_R	3000 ± 300	3300 ± 200
γ_2	3.16 ± 0.08	3.10 ± 0.03
χ^2	1.2	1.1

lution of the parameterized equation (4) are presented in Table 2 at the QGSJET and SIBYLL interaction models. As it is seen from Fig. 11 and Tables 1,2, the derived expected primary energy spectra significantly depend on interaction model. The expected abundance of primary nuclei at energy $E \sim 10^3$ TeV in the framework of SIBYLL model agrees well with corresponding extrapolations of the balloon and satellite data [21], whereas the predictions according to the QGSJET model point out to a predominantly proton primary composition in the $10^3 \div 10^5$ TeV energy range.

VII. EVENT-BY-EVENT ANALYSIS

The mountain location of the GAMMA experiment and the agreements of observed and simulated data in the measurement range $5 \cdot 10^5 \leq N_{ch} < 10^7$ (Fig. 4-10) allowed, apart from above, to obtain the all-particle energy spectra with high reliability. The method is based on an event-by-event evaluation of primary energy using the reconstructed parameters $\tilde{N}_{ch}, \tilde{N}_\mu, \tilde{s}, \theta$ of detected

EAS. Such possibilities have been studying for a long time in different papers [10, 29, 30] and the main difficulty was to obtain an unbiased energy estimation at an existent abundance of the primary nuclei taking into account the fluctuations of shower development and detector response.

Using the simulated database, $J = 1.5 \cdot 10^4$ EAS events were taken for each of $k = 1, \dots, 4$ kinds (H, He, O, Fe) of primary nuclei and each interaction model (SIBYLL, QGSJET). The reconstructed $\tilde{N}_{ch}, \tilde{N}_\mu, \tilde{s}$ shower parameters, known zenith angle θ and primary energy E_0 were used at minimization

$$\chi^2(a_1, \dots, a_p) = \frac{1}{4J} \sum_{k=1}^4 \sum_{j=1}^J \frac{(\ln E_{1,k,j} - \ln E_{0,k,j})^2}{\sigma_E^2} \quad (5)$$

where $E_1 = f(a_1, \dots, a_p | \tilde{N}_{ch}, \tilde{N}_\mu, \tilde{s}, \theta)$ is the investigated parametric function with a_1, \dots, a_p parameters, σ_E is expected accuracy of the E_1 evaluated energy. The best

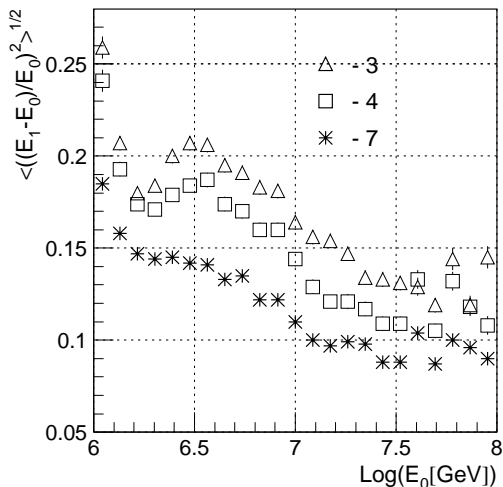


FIG. 12: Accuracy (RMSD) of the primary energy evaluations at different number of approximation parameters.

estimations were achieved at 7-parametric ($p = 7$) fit:

$$\ln E_1 = a_1 x + \frac{a_2 s}{c} + a_3 + a_4 c + a_5 e^s + \frac{a_6}{(x - a_7 y)}, \quad (6)$$

where $x = \ln \tilde{N}_{ch}$, $y = \ln \tilde{N}_\mu$ ($R < 50m$), $c = \cos \theta$ and energy E_1 has units of GeV. The values of the a_1, \dots, a_7 parameters for both interaction models and the corresponding χ^2 obtained from (5) at $\sigma_E = 0.15$ are displayed in Table 3. The root mean square deviations of the energy estimation by 7-parametric fit (4) in the framework of the SIBYLL model is shown in Fig. 12. The corresponding results at three (only x, \tilde{s} variables) and 4-parametric ($x, \tilde{s}, \cos \theta$) fit are shown in Fig. 12 as well.

The obtained error distributions estimating primary energy by 7-parametric approximation (6), are shown in Fig. 13 for H, He, O, Fe nuclei. The red line corresponds

TABLE III: Approximation parameters a_1, \dots, a_7 of primary energy evaluation (6) and corresponding χ^2 obtained from (6) at the SIBYLL and QGSJET interaction models.

Model	a_1	a_2	a_3	a_4	a_5	a_6	a_7	χ^2
SIBYLL	1.03	3.98	-4.3	2.01	-1.2	11.8	0.94	0.85
QGSJET	1.03	4.38	-4.6	2.35	-1.3	11.5	0.96	0.94

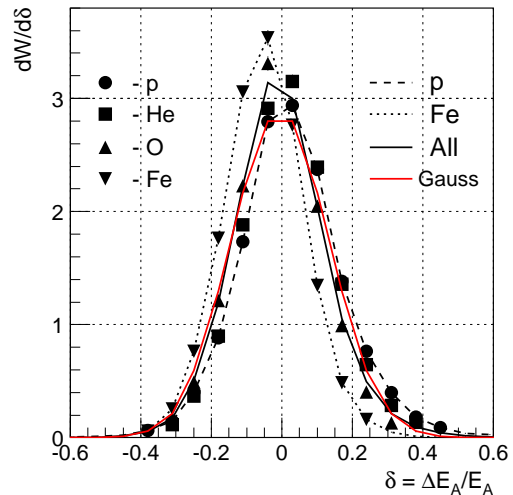


FIG. 13: Distribution of errors of the primary energy estimation by event-by-event 7-parametric fit at different primary nuclei.

to the Gaussian distribution at the same parameters as cumulative distribution (black solid line).

The all-particle energy spectrum derived on the basis of the GAMMA 2002-2004 EAS data set and fit (6), at the QGSJET (filled red square symbols) and SIBYLL (filled blue circle symbols) interaction models are shown in Fig. 14.

Notice, that the energy spectrum obtained by event-by-event method claims additional corrections, because the errors $\sigma_E = \sigma(\Delta E/E)$ and power-law energy spectra ($\sim E^{-\gamma}$) lead to an overestimation of the spectrum $\eta = \exp(((\gamma - 1)\sigma_E)^2/2)$ times. Moreover, the inevitable biases of energy estimations $\epsilon(A) = \langle E_1/E_0 \rangle$ depend on primary nuclei and shift the corresponding energy spectra $\beta(A) = \epsilon^{\gamma-1}$ times. The spectral shift due to $\beta(A) \neq 1$ impossible to take into account without information about abundance of primary nuclei.

The observed biases of 7-parametric fit (6) are distributed from $\epsilon(p) \simeq 1.02\%$ up to $\epsilon(Fe) \simeq 0.96\%$ (Fig. 13) and here are neglected. In the results shown in Fig. 14, the corrections of $\eta(E)$ are taken into account using the expected accuracies from Fig. 12.

The solid (red) and dashed (blue) lines in Fig.14 represent the all-particle primary energy spectra obtained on the basis of GAMMA data set by the solution of parametrized EAS inverse problem in the framework of the SIBYLL and QGSJET models respectively. The

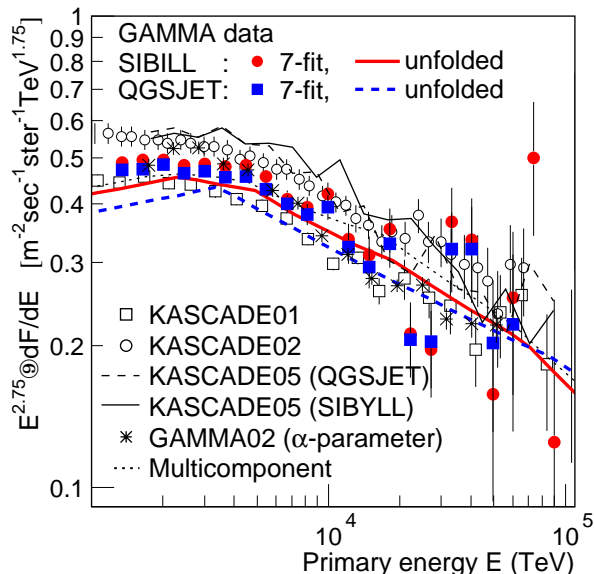


FIG. 14: All particle primary energy spectra obtained by event-by-event 7-parametric analysis (filled symbols) and EAS inverse problem solutions (solid and dashed lines) on the basis of GAMMA 2002-2004 database.

event-by-event analysis of the GAMMA data at the QGSJET interaction model using α -parametric method [10] also shown in Fig. 14 (asterisk symbols). The dotted line in Fig. 14 represents the parametrized solutions of the EAS inverse problem for the KASCADE EAS data at rigidity-dependent steepening primary energy spectra [28]. The results of KASCADE02 in Fig. 14 obtained by the non-parametric event-by-event analysis was taken from review [31]. The KASCADE01,05 data obtained by the iterative method [33] of unfolding of the EAS inverse problem were taken from [20, 32] respectively.

VIII. CONCLUSION

The self-consistency of results (Fig. 2-10) obtained by GAMMA experiment at least up to $N_{ch} \simeq 10^7$ and corresponding predictions in the framework of hypothesis of the rigidity-dependent steepening primary energy spectra and validity of the SIBYLL or QGSJET interaction models point towards:

- The anomalous behavior of the EAS muon spectra

(overestimation, Fig. 4b,8,10) and EAS age parameter at EAS size $N_{ch} > 10^7$. The same behavior of the EAS age parameter had been observed also in [15, 22].

- The obtained abundances and energy spectra of primary p, He, O, Fe nuclei depend on interaction models. The SIBYLL interaction model is more preferable in terms of the extrapolation of the derived expected primary spectra (Fig. 11) to the energy range of the direct measurements.
- The rigidity-dependent steepening energy spectra of primary nuclei describe the EAS data of the GAMMA experiment at least up to $N_{ch} \simeq 10^7$ with average accuracy $< 10\%$ at particle's magnetic rigidity $E_R \simeq 2400 \div 3000$ TV (SIBYLL) and $E_R \simeq 3300 \pm 200$ TV (QGSJET).
- The 4-dimensional approach at the EAS inverse problem solution is more preferable in terms of the stability and accuracies of solutions.
- The obtained all-particle energy spectra slightly depend on interaction model and are practically the same at both the event-by-event reconstruction method and the EAS inverse approach.

The obtained energy spectra of primary nuclei ($A \equiv p, He, O, Fe$) in the energy range $10^6 < E_A < 5 \cdot 10^7$ GeV disagree (see Fig. 11) with the same KASCADE data obtained by the iterative method [33]. However, the discrepancies of all-particle energy spectra (see Fig. 14) obtained by the GAMMA and KASCADE experiments are sufficiently small ($\sim 20\%$).

Acknowledgments

We are grateful to all of our colleagues at the Moscow Lebedev Institute and the Yerevan Physics Institute who took part in the development and exploitation of the GAMMA array.

This work has been partly supported by research grant No 1465 from the Armenian government, NFSAT bilateral U.S.-Armenian grant AS084-02/CRDF 12036, by the CRDF grant AR-P2-2580-YE-04 and the "Hayastan" All-Armenian Fund in France.

[1] B. Peters, Nuovo Cim. (Suppl.) **14**,(1959) 436.
 [2] P.L. Biermann, Astron. & Astrph. **271** (1993).
 [3] T. Stanev, P.L. Biermann, T.K. Gaisser, Astron. Astrophys. **274** (1993) 902 .
 [4] T. Antoni et al., Nucl. Instr. & Meth. A 513 (2003) 490.
 [5] M. Aglietta et al., Astropart. Phys. **10** (1999) 1.

[6] M.A.K. Glasmacher et al., Astropart. Phys. **10** (1999) 291.
 [7] T.V. Danilova, E.A. Danilova, A.B. Erlykin et al., Nucl. Instr. & Meth. A323 (1992) 104.
 [8] V.S. Eganov, A.P. Garyaka et al., J. Phys G:Nucl. Part. Phys. **26** (2000) 1355.

- [9] M.Z. Zazyan, A.P. Garyaka, R.M. Martirosov and J. Procureur, Nucl. Phys. B (Proc.Suppl.) **97** (2001) 294.
- [10] A.P. Garyaka, R.M. Martirosov, J. Procureur et al., J. Phys G:Nucl. Part. Phys. **28** (2002) 2317.
- [11] V.S. Eganov, A.P. Garyaka, L.W. Jones et al., Proc. 28th Intern. Cosmic Ray Conf. Tsukuba, HE1.1 (2003) 49.
- [12] R.S. Fletcher, T.K. Gaisser, P. Lipari, T. Stanev, Phys.Rev. D **50** (1994) 5710.
- [13] N.N. Kalmykov, S.S. Ostapchenko, Yad. Fiz. **56** (1993) 105 (in Russian).
- [14] V.V. Avakian, O.S. Babadjanian et al., Preprint YERPHI-1167(44)-89, Yerevan (1989).
- [15] V.V. Avakian et al., Proc. 24th Intern. Cosmic Ray Conf., Rome **1** (1995) 348.
- [16] S.V. Ter-Antonyan Preprint YERPHI-1168(45)-89, Yerevan (1989).
- [17] D. Heck, J. Knapp, J.N. Capdevielle, G. Schatz, T. Thouw, Forschungszentrum Karlsruhe Report, FZKA 6019 (1998) 90 p.
- [18] R. Glasstetter et al. Proc. 26th Inter. Cosmic Ray Conf. Salt Lake City **1** (1999) 222.
- [19] S.V. Ter-Antonyan and P.L. Biermann, Proc. 27th Intern. Cosmic Ray Conf., Hamburg (2001) HE054 1051 (astro-ph/0106091).
- [20] H. Ulrich et al., Proc. 27th Intern. Cosmic Ray Conf., Hamburg **1** (2001) 97.
- [21] B. Wiebel-Sooth and P. Biermann, Preprint Max-Planck Inst. für Radioastr., Bonn, No.772, (1998)/ B. Wiebel-Sooth et al., Proc. 24th Inter. Cosmic Ray Conf. Rome **1** (1995) 482.
- [22] S. Miyake, N. Ito et al., Proc. 16th Intern. Cosmic Ray Conf., Kyoto **13** (1979) 171.
- [23] D. Adamov et al., Proc. 20th Intern. Cosmic Ray Conf. Moscow **5** (1987) 460.
- [24] N. Nagano, T. Hara et al., J. Phys. G:Nucl. Phys. **10** (1984) 1295.
- [25] K.-H. Kampert, astro-ph/0405608 v1 (2004).
- [26] Samvel Ter-Antonyan, 28th Intern. Cosmic Ray Conf. Tsukuba HE2 (2003) 239.
- [27] G. Schatz, Astropart. Phys. **17** (2002) 13.
- [28] Samvel Ter-Antonyan and Peter Biermann, 28th Intern. Cosmic Ray Conf. Tsukuba HE1 (2003) 235.
- [29] J.-N. Capdevielle et al., Proc. 27th Inter. Cosmic Ray Conf., Hamburg (2001) 306.
- [30] A. Chilingaryan, S. Ter-Antonyan et al, Nucl. Phys.B **60B** (1998) 117.
- [31] S.P. Swordy, L.F. Fortson et al., Astropart. Phys. **18** (2002) 129.
- [32] T. Antoni et al., astro-ph/0505413 v1 (2005) (accepted in Astropart. Phys.)
- [33] R. Gold, ANL-6984 Report, Argonne (1964).